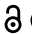




RESEARCH PAPER

 OPEN ACCESS 

Dengue virus strain 2 capsid protein switches the annealing pathway and reduces intrinsic dynamics of the conserved 5' untranslated region

Xin Ee Yong ^{a,b}, Palur Venkata Raghuvamsi^c, Ganesh S. Anand^c, Thorsten Wohland^{b,c}, and Kamal K. Sharma^{b,c}

^aNUS Graduate School for integrative Sciences and Engineering Programme, National University of Singapore, Singapore; ^bCentre for Bioimaging Sciences, National University of Singapore, Singapore, Singapore; ^cDepartment of Biological Sciences, National University of Singapore, Singapore, Singapore

ABSTRACT

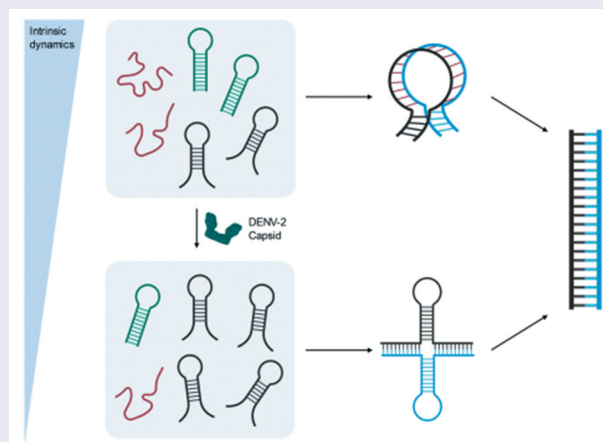
The capsid protein of dengue virus strain 2 (DENV2C) promotes nucleic acid structural rearrangements using chaperone activity. However, the role of DENV2C during the interaction of RNA elements in the conserved 5' untranslated region (5'UTR) to the 3' untranslated region (3'UTR) is still unclear. Thus, we investigated the effect of DENV2C on the annealing mechanism of two RNA hairpin elements from the 5'UTR to their complementary sequences during (+)/(-) ds-RNA formation and (+) RNA circularization. DENV2C was found to switch the annealing pathway for RNA elements involved in (+)/(-) ds-RNA formation, but not for RNA elements related to (+) RNA circularization. In addition, we also determined that DENV2C modulates intrinsic dynamics and reduces kinetically trapped unfavourable conformations of the 5'UTR sequence. Thus, our results provide mechanistic insights by which DENV2C chaperones the interactions between RNA elements at the 5' and 3' ends during genome recombination, a prerequisite for DENV replication.

ARTICLE HISTORY

Received 2 September 2020
Revised 17 November 2020
Accepted 2 December 2020

KEYWORDS

RNA chaperone; FRET-FCS; genome circularization; RNA replication; kissing loop




Introduction

Dengue fever is caused by infection with dengue virus (DENV), which is transmitted by the bite of *Aedes aegypti* or *Aedes albopictus* mosquitoes carrying the virus. DENV has four antigenically-distinct serotypes, DENV1–4, which complicate vaccine development because an effective vaccine should neutralize all four serotypes effectively [1]. This is essential because secondary dengue infection tends to cause severe symptoms, such as dengue haemorrhagic fever and can even be fatal [2].

DENV2 is a positive-sense single-stranded RNA (ssRNA) virus with an icosahedral structure ($T = 3$). The 50 nm virus

has a genome of approximately 10.7 kb, which is translated to a polypeptide that is cleaved into three structural (envelope [E], pre-membrane [prM] and capsid [C]) and seven non-structural proteins (NS1, NS2A, NS2B, NS3, NS4A, NS4B, NS5) [3]. The coding region is flanked at both ends by untranslated regions (UTR). The 5' end has a type I cap structure ($m^7GpppAmp$) mediating cap-dependent translation, but the virus can switch to a noncanonical translation mechanism when translation factors are limiting [4]. Circularization of the (+) RNA genome is found to be essential for viral replication as mutations in conserved circularization RNA sequences reduces viral fitness [5,6]. This (+) RNA

CONTACT Kamal K. Sharma  dbskks@nus.edu.sg; Thorsten Wohland  twohland@nus.edu.sg  Centre for Bioimaging Sciences, National University of Singapore, Singapore 117557, Singapore

 Supplemental data for this article can be accessed [here](#).

© 2021 The Author(s). Published by Informa UK Limited, trading as Taylor & Francis Group. This is an Open Access article distributed under the terms of the Creative Commons Attribution License (<http://creativecommons.org/licenses/by/4.0/>), which permits unrestricted use, distribution, and reproduction in any medium, provided the original work is properly cited.

circularization of the DENV genome (Fig. 1A) is proposed to proceed either through protein-nucleic acid interactions [6] or via long range RNA-RNA-based 5' and 3' (5'-3') end interactions, which can occur in the absence of proteins [7–12]. Thus far, two complementary RNA elements at the 5' and 3' ends have been identified for such long range 5'-3' RNA end interactions and are necessary for (+) RNA circularization [8]. One of these sequences, a hairpin structure, known as the 5' upstream AUG region (5'UAR) element in the 5'UTR, anneals with its complementary 3'UAR counterpart, which is located at the bottom of 3' stem loop (3'SL) in the 3'UTR (Fig. 1B) [7,9,12]. In addition to the RNA sequences involved in 5'-3'-end interactions necessary for the (+) RNA circularization, the 5' end of the viral genome harbours another functional RNA element capsid-coding region hairpin (5'cHP). The 5'cHP element resides within the capsid-coding region and directs start codon selection for RNA translation [13,14]. It is believed that the 5'cHP stalls the scanning initiation complex over the first AUG, favouring its recognition [15] and stabilizing the overall 5'-3' panhandle structure [13]. (+) RNA circularization is also essential for the synthesis of the DENV (-) RNA genome, which serves as template for the amplification of (+) RNA which can be packaged to synthesize new virions [12]. This (-) RNA genome synthesis includes NS5 binding at the 5'UTR and relocation of the polymerase at the 3' initiation site via the (+) RNA circularization [8,16]. Thus, the hybridization of these complementary RNA elements at 5' and 3' ends are speculated to play a dual role during DENV transcription: (i) to bring the NS5 polymerase-5'UTR promoter complex near the 3' end of the genome and (ii) to open the large stem of the 3'SL structure by 5'-3'UAR annealing [17]. Furthermore during (-) RNA genome synthesis, secondary structures of the conserved 5'UTR RNA elements, like 5'UAR and 5'cHP, which are templates for (-) RNA synthesis, melts and form double-stranded (+)/(-) RNA (ds-RNA) by annealing to their complementary (-) RNA sequences, c5'UAR and c5'cHP, respectively (Fig. S1A and C) [13]. The stem-loop structure of 5'UAR melts during both (+) RNA circularization as well as during (-) RNA synthesis, while the structure of 5'cHP melts only during (-) RNA synthesis, thus emphasizing the role of 5'UAR in stabilizing the circular over the linear form of DENV genome (Fig. 1A) [18].

Furthermore, both (+)/(-) ds-RNA formation and the (+) RNA circularization require the aid of RNA chaperones. RNA chaperones help to prevent misfolding of RNA by allowing RNA to sample many different conformations [19]. The DENV2 capsid protein, DENV2C, promotes annealing of the hammerhead ribozyme to its substrate, and promotes dissociation of the cleaved substrates, demonstrating RNA chaperoning ability [20]. DENV2C exists as a homodimer, consisting of two 100-aa subunits. The 13 kDa DENV2C is highly basic, containing 26/100 basic amino acids and has a flexible disordered region in the N-terminus, both key characteristics of many RNA chaperones (Fig. 1C) [21–24]. The protein associates with the ssRNA genome to form the nucleocapsid and encapsulates the nucleocapsid in a lipid bilayer containing E and

M proteins [25]. DENV2C binds to RNA via its basic residues in helix-4 while binds to lipid bilayer using its hydrophobic cleft in helix-1 [26,27]. All further reference to DENV2C would be to one unit of the protein, i.e. the monomer.

Considering the abovementioned facts, DENV2C plays a vital role during virus formation possibly by modulating the interplay of RNA elements in the virus genome. Although the interaction of RNA elements in the DENV 5' and 3' ends is required for viral RNA replication, the role of DENV2C during this interplay is still not explored. We hypothesize that, due to its chaperone properties, the DENV2C is involved in genome rearrangements that are essential to RNA replication and viral fitness by modulating the annealing mechanism of the RNA element, 5'UAR, during (+)/(-) ds RNA formation and (+) RNA circularization.

To achieve this, we characterized the role of DENV2C as an RNA chaperone by investigating the annealing kinetics of 21-nt 5'UAR and 23-nt 5'cHP to their complementary sequences in the context of (+)/(-) ds-RNA formation and (+) RNA circularization. To represent the (-) RNA synthesis or (+)/(-) ds-RNA formation, we investigated annealing kinetics of the 21-nt long 5'UAR and 23-nt long 5'cHP with their complementary c5'UAR and c5'cHP, respectively (Fig. 1B). On the other hand, the (+) RNA circularization event is modelled by the annealing of 21-nt long 5'UAR with its complementary 3'UAR counterpart (Fig. 1B), which is located at the bottom part of 3'SL of the viral RNA. We doubly labelled 5'UAR and 5'cHP with 6-carboxyfluorescein (FAM) as the donor fluorophore at the 5' end and carboxytetramethylrhodamine (TAMRA) as the acceptor fluorophore at the 3' end, forming a Förster resonance energy transfer (FRET)-pair. Due to the proximity of donor and acceptor dyes in hairpin conformation of both 5'UAR and 5'cHP, the fluorescence of FAM is quenched. With the addition of a complementary sequence, the hairpin converts into a double-stranded sequence (extended duplex), in turn increasing the distance between donor and acceptor fluorophores. This increase in distance leads to fluorescence recovery of the donor that will provide information about the real-time annealing kinetics. By monitoring the annealing kinetics of the native and mutated 5'UAR and 5'cHP, we found that DENV2C promotes all three 5'UAR/c5'UAR, 5'cHP/c5'cHP and 5'UAR/3'UAR annealing. Interestingly, DENV2C is also able to switch the 5'UAR/c5'UAR annealing pathway that predominantly nucleates via the hairpin loops to a reaction pathway, nucleating through the hairpin stems. However, DENV2C does not alter the 5'UAR/3'UAR annealing pathway. We also determined by using FRET-fluorescence correlation spectroscopy (FRET-FCS) and time-resolved FRET (trFRET) that DENV2C exerts its chaperone functioning by reducing intrinsic dynamics of the 5'UAR and probably favouring one of the active conformations of the RNA hairpin. We also proposed mechanisms for 5'UAR/c5'UAR and 5'UAR/3'UAR annealing and compared the effects of DENV2C on (+)/(-) ds-RNA formation and (+) RNA circularization. Overall, our results provide the reaction mechanism by which DENV2C modulates the annealing of the 5'UAR sequence during (+)/(-) ds RNA formation and (+) RNA circularization, revealing how DENV2C can play a role in genomic rearrangements of 5'UAR that are essential to RNA replication and DENV fitness.

Materials and methods

Oligonucleotides

All oligoribonucleotides (ORN) were synthesized by Integrated DNA Technologies (Singapore). The doubly labelled ORNs (5'UAR, 5'UAR-ULoop, 5'cHP and 5'cHP-ULoop) were synthesized with 6-carboxyfluorescein (FAM) at the 5' end and carboxytetramethylrhodamine (TAM) at the 3' end. All ORNs were purified by the manufacturer using HPLC.

DENV2C protein synthesis and purification

pET-21a(+) vector containing DENV2C protein gene sequence with N-terminal His tag and Tobacco Etch Virus (TEV) digestion site was purchased from GenScript (China). Recombinant capsid protein from DENV2 NGC strain was expressed in *Escherichia coli* BL21 strain. Transformed cells were grown in Luria-Bertani (LB) media supplemented with ampicillin (100 µg/ml) at 37°C until an optical density, OD₆₀₀ of 0.6–0.8 was reached. A final concentration of 1 mM of isopropyl β-D-1-thiogalactopyranoside (IPTG) was used to induce expression and incubated for 16 to 18 hours at 18°C. This overnight culture was harvested by centrifugation at 6000 x g for 15 minutes at 4°C. The cells were lysed by sonication in NTE buffer consisting of 50 mM Tris-HCl, 1 M NaCl, pH 7.5 with 0.8 mM DTT, protease inhibitor cocktail (COEDTAF-RO, Merck) and 40 µg/ml of RNase A (Thermo Fisher Scientific). The cell pellet was separated by centrifugation at 13,000 rpm for 30 minutes, and the supernatant was collected and incubated with Cobalt beads for affinity chromatography. DENV2C protein was eluted at 1 M imidazole in NTE buffer and the collected elute was subjected to size exclusion chromatography (HiLoad 16/600 Superdex 200, GE Healthcare). The fraction containing DENV2C protein were pooled and dialysed against 50 mM HEPES, 150 mM NaCl, pH 7.5 buffer to remove imidazole and reduce NaCl concentration. Dialysed DENV2C protein was concentrated using Amicon Ultra-4 Centrifugal Filter Units (10 kDa molecular weight cut off, Millipore). The concentration of the purified protein sample was determined using nanodrop. DENV2C protein preparations were ribonuclease-free (Fig. S2) and RNA-free, determined by a A260/A280 value of 0.7 for the purified protein, very close to the theoretical value of 0.57 for a protein sample not contaminated by nucleic acids.

Fluorescence spectroscopy

Fluorescence spectroscopy measurements were done on Cary Eclipse Fluorescence Spectrophotometer (Agilent) with a temperature control module, using Hellma® fluorescence cuvettes with an internal chamber volume of 45 µL. Excitation and emission wavelengths of 480 nm and 520 nm were used to track the intensity of 5' FAM on doubly labelled ORNs in real-time. Reactions were done in pseudo first order conditions, with the concentration of non-labelled ORN being at least 10-fold more than the doubly labelled ORN. Equal volumes of both reactants were mixed at the start of the

reaction to prevent high local concentrations of either reactant. For reactions in the presence of DENV2C, the protein was added to each ORN and mixed well before the two reactants were mixed. DENV2C:ORN ratios of 2:1 was used for all reactions in the presence of DENV2C protein. All reactions were done in 50 mM HEPES, 30 mM NaCl, 0.2 mM MgCl₂, pH 7.5 buffer and at 20°C, unless otherwise stated. Temperature-dependence experiments to obtain Arrhenius parameters were done by equilibrating both reactants at the specified temperature for 10 minutes prior to mixing. All curve fitting was done on OriginPro™ software (ver 9.55).

FCS and FRET-FCS

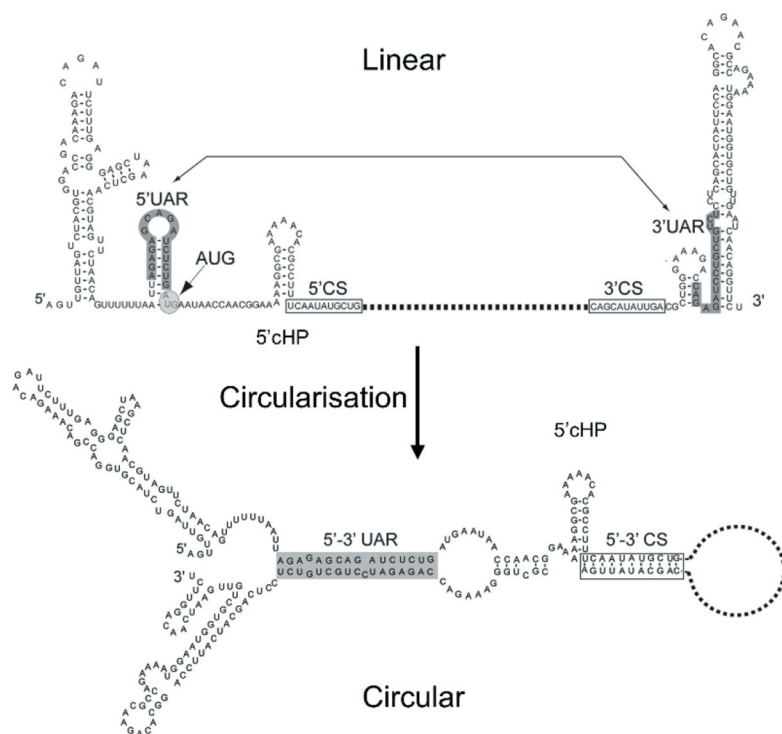
FCS measurements were carried out on a commercial Olympus FV1200 laser scanning confocal microscope (Olympus, Singapore) equipped with an FCS upgrade kit (PicoQuant, Berlin, Germany). Doubly labelled ORN samples were excited with a 543 nm continuous wave laser. The beam was focused onto the sample by a water immersion objective (60×, NA 1.2; Olympus, Singapore) after being reflected by a dichroic mirror (DM405/485/543/635, Olympus, Singapore) and the scanning unit. The 3'TAMRA fluorescence from 5'UAR was recorded by a single molecule avalanche photodiode (SPAD) (SPCM-AQR-14, PerkinElmer Optoelectronics, Quebec, Canada), through a 600/50 band pass emission filter. Detected photon counts are registered by a TimeHarp 260 time-correlated single photon counting board (PicoQuant). Autocorrelation analysis was done using SymPhoTime 64 (PicoQuant, Berlin, Germany) to obtain diffusion time and number of fluorescent particles. ORN and DENV2C protein mixtures were incubated for 10 minutes before measurements. All measurements were performed at room temperature.

For FRET-FCS, the fluorescence signal from doubly-labelled 5'UAR was spectrally divided into donor and acceptor channels by a 560 dichroic longpass (DCLP) mirror. The donor and acceptor fluorescence were recorded using a set of single-molecule avalanche photodiodes (SPADs) (SPCM-AQR-14, PerkinElmer Optoelectronics, Quebec, Canada), through a 513/17 and 615/45 band pass emission filter (Omega, VT), respectively. The intensities of the donor and acceptor channel are collated in 20 µs time bins in the SymPhoTime64 software and exported. Using a home-written MATLAB script, the proximity ratio was calculated for each time bin and the autocorrelation of the proximity ratio was calculated. The calculated autocorrelation of the proximity ratio was then fitted using the Levenberg-Marquardt iteration algorithm by Origin 9.1.

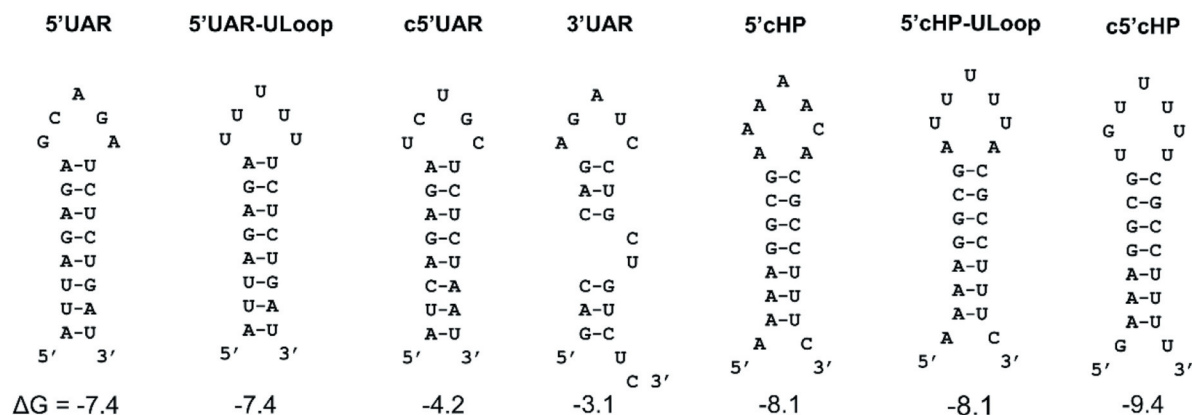
Time-resolved FRET (trFRET)

trFRET measurements were carried out on the same commercial Olympus FV1200 laser scanning confocal microscope equipped with a time-resolved LSM upgrade kit (Microtime 200, PicoQuant, GmbH, Berlin, Germany). Doubly labelled 5'UAR ORN was excited with a 485 nm pulsed diode laser with a 20 MHz repetition rate and 29 mW power (PDL series, Sepia II combiner module). The beam was focused into the sample by a water immersion objective (60×, NA 1.2;

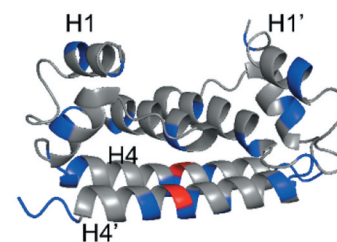
A DENV genome



B Oligonucleotides



C DENV2C protein



MNDQRKKARNTPFNMLKRER
 NRVSTVQQLTKRFLGMLQGR
 GPLKLFMALVAFRLFLTIPPTA
 GILKRWGTIKKSKAINVLRGF
 RKEIGRMLNILNRRRR

Figure 1. Structure of (A) DENV genome (adapted from [64]), (B) ORN sequences used in this study, and (C) DENV2C protein (PDB: 1R6R). (A) The 5' and 3' UTR region of DENV genome contain conserved circularization sequences, 5'-3' UAR (upstream AUG region) (grey). Annealing of these circularization sequences allow the formation of the circularized genome. (B) ORN sequences are derived from the 5'UAR, 5'cHP and 3'UAR region of the genome. Their secondary structures and ΔG values, shown below the structures in kcal/mol, were predicted using the mfold webtool (<http://unafold.rna.albany.edu/>). 5'UAR, 5'UAR-ULoop, 5'cHP and 5'cHP-ULoop are doubly labelled with 5' FAM and 3' TAMRA. Annealing pairs 5'UAR/c5'UAR and 5'cHP/c5'cHP represent (+)/(-) ds RNA, whereas 5'UAR/3'UAR are representing the (+) RNA circularization event. (C) The DENV2C protein is a homodimer. Blue and red residues highlight basic and acidic residues, respectively. The $\alpha 1$ helix (H1) and $\alpha 4$ helix (H4) are labelled for both subunits of the protein, with H1 and H4 from one subunit and H1' and H4' from the other subunit. In the protein sequence of DENV2C monomer, residues in red are part of the N-terminus disordered region which are not shown in the structure.

Olympus, Singapore) after being reflected by a dichroic mirror (DM405/485/543/635, Olympus, Singapore) and the scanning unit. The fluorescence was collected by the same objective followed by a pinhole (120 mm) to remove out-of-focus light. The fluorescence signal was spectrally divided into donor (green) and acceptor (red) channels by a 560 DCLP mirror. The 5'FAM donor fluorescence was recorded by a SPAD (SPCM-AQR-14, PerkinElmer Optoelectronics,

Quebec, Canada), through a 513/17 band pass emission filter (Omega, VT). This donor signal was further processed by a time correlated single photon counting card (TimeHarp 260, PicoQuant) to build up the histogram of photon arrival times. The trFRET measurements were recorded for 180 s after incubating 5'UAR and DENV2C samples for 10 min at room temperature. The mean lifetime (τ) was calculated from the individual fluorescence lifetimes (τ_i) and their

relative amplitudes (a_i) according to $(\tau) = \sum^{\alpha_i} \tau_i$. Donor fluorescence lifetime decay data were treated using the software SymPhoTime 64 (PicoQuant, GmbH). In all cases, the χ^2 values were close to 1 and the weighted residuals as well as their autocorrelation were distributed randomly around 0, indicating a good fit. The reported values are mean and S. D.'s from at least three replicates.

Results

5'UAR/c5'UAR and 5'cHP/c5'cHP annealing is faster than 5'UAR/3'UAR annealing

Annealing kinetics of doubly labelled 5'UAR to its non-labelled c5'UAR were monitored by tracking the increase in FAM fluorescence (Fig. 2A). Comparing the emission spectra of doubly labelled 5'UAR at the start and end of the annealing reaction shows a decrease in FRET with the formation of the extended duplex (Fig. 3A) as seen by an increase in FAM fluorescence and a corresponding decrease in TAMRA fluorescence. The real-time fluorescence intensity traces of the 5'UAR/c5'UAR reaction kinetics were fitted to a biexponential equation (1), where $I(t)$ is the actual fluorescence intensity at 520 nm, upon excitation at 480 nm, $k_{\text{obs}1}$ and $k_{\text{obs}2}$ are the pseudo first order fast and slow reaction rates, a is the relative amplitude of the fast component and t_0 is the start time of the reaction. I_0 and I_f is the fluorescence intensity of doubly-labelled 5'UAR in the free state and in the final extended duplex (ED), respectively.

$$I(t) = I_f - (I_f - I_0) \left(a e^{-k_{\text{obs}1}(t-t_0)} + (1-a) e^{-k_{\text{obs}2}(t-t_0)} \right) \quad (1)$$

The fast and slow reaction rates, $k_{\text{obs}1}$ and $k_{\text{obs}2}$, were plotted against the concentration of non-labelled reactant, c5'UAR (Fig. 2D and 2G). The fast component, $k_{\text{obs}1}$, linearly varies with increasing c5'UAR concentrations ($[c5'UAR]$), while the slow component, $k_{\text{obs}2}$, shows a hyperbolic dependence. The linear relationship between $k_{\text{obs}1}$ and $[c5'UAR]$ follows Equation (2) [28].

$$k_{\text{obs}1} = k_{\text{ass}}[c5'UAR] + k_{\text{diss}} \quad (2)$$

The hyperbolic dependence of $k_{\text{obs}2}$ on increasing $[c5'UAR]$ can be described in Equation (3), where K_a is the equilibrium constant governing intermediate complex (IC) formation, k_f and k_b are forward and backward interconversion kinetic rate constants.

$$k_{\text{obs}2} = \frac{k_f K_a [c5'UAR]}{1 + K_a [c5'UAR]} + k_b \quad (3)$$

Fitting the linear and hyperbolic plots of $k_{\text{obs}1}$ and $k_{\text{obs}2}$ against increasing $[c5'UAR]$ with Equations (2) and (3), respectively, generated kinetic parameters shown in Table 1.

Based on our acquired kinetic parameters, a reaction mechanism with single kinetic pathway starting from a 5'UAR species can be proposed:

where a fast pre-equilibrium intermediate complex, $IC_{5'UAR}$, precedes the formation of the final stable extended duplex, $ED_{5'UAR}$, through a monomolecular reaction [29]. The formation of $IC_{5'UAR}$ is governed by the second order

association constant, k_{ass} , and the first order dissociation constant, k_{diss} , whereas the formation of $ED_{5'UAR}$ is governed by the forward and backward interconversion kinetic rate constants, k_f and k_b , respectively. The hyperbolic dependence of $k_{\text{obs}2}$ with increasing $[c5'UAR]$ can be attributed to $IC_{5'UAR}$ accumulation because of its slow interconversion to $ED_{5'UAR}$. This is likely the rate-limiting step of the 5'UAR/c5'UAR annealing.

The k_{ass} value of $50 (\pm 3) M^{-1}s^{-1}$ for 5'UAR/c5'UAR annealing is at least 4 orders of magnitude smaller than the rate constants reported for annealing of unstructured sequences (10^5 – $10^7 M^{-1}s^{-1}$), suggesting that there is a low probability for the reaction to occur at room temperature [30]. The k_{diss} and k_b values were $3.6 (\pm 0.7) \times 10^{-4} s^{-1}$ and close to zero, respectively, suggesting that dissociation of both $IC_{5'UAR}$ and $ED_{5'UAR}$ is negligible (Table 1).

To validate the postulated annealing mechanism [31–34], we used the Dynafit numerical resolution software [35], which allows simultaneous fitting of the experimental progress curves obtained at different $[c5'UAR]$ (Fig. S3). The best estimates of the elementary rate constants k_{ass} , k_{diss} and k_f (Table S1) were in excellent agreement with those found by the empirical approach (Table 1).

Further insights into the nature of 5'UAR/c5'UAR annealing pathway were obtained from determining the temperature dependence of k_{obs} values, using the Arrhenius equation (4), which can be rewritten in a linear form [5], where the rate constant k is given by $k_{\text{obs}}/[c5'UAR]$, A is the pre-exponential Arrhenius factor, E_a is the activation energy, R is the universal gas constant and T is the temperature (in Kelvin).

$$k = A e^{-\frac{E_a}{RT}} \quad (4)$$

$$\ln \frac{k_{\text{obs}}}{[c5'UAR]} = \ln A - \frac{E_a}{R} \left(\frac{1}{T} \right) \quad (5)$$

We observed an increase in both reaction rates leading to positive enthalpy values of the transition states of $11.9 (\pm 0.4) \text{ kcal/mol}$ and $18.0 (\pm 1.0) \text{ kcal/mol}$ for the fast and the slow components, respectively (Fig. 4 and Table 2). This suggests a pre-melting of 2–3 base-pairs (bp) of hydrogen bonds in 5'UAR hairpin structure [36,37].

Next, similar to 5'UAR/c5'UAR annealing, 5'cHP/c5'cHP annealing shows a linear and hyperbolic dependence of $k_{\text{obs}1}$ and $k_{\text{obs}2}$ values against increasing $[c5'cHP]$ (Fig. S4), thus suggesting a similar reaction mechanism as to that proposed by Scheme 1 (shown by Scheme a in the supplementary). The formation of IC_{cHP} was found to be ~ 1.7 -fold faster in 5'cHP/c5'cHP annealing compared to 5'UAR/c5'UAR annealing with k_{ass} values of $85 (\pm 5) M^{-1}s^{-1}$ and $50 (\pm 3) M^{-1}s^{-1}$, respectively (Table 1). However, the interconversion from IC_{cHP} to ED_{cHP} is slower by ~ 4 -fold for 5'cHP/c5'cHP annealing compared to that of 5'UAR/c5'UAR annealing (Table 1), which can be attributed to the greater stability of the 5'cHP hairpin, with a ΔG_{cHP} of -8.1 kcal/mol compared to a $\Delta G_{5'UAR}$ of -7.4 kcal/mol (Fig. 1).

As mentioned earlier, investigating 5'UAR/3'UAR annealing will provide insights about (+) RNA circularization. Interestingly, 5'UAR/3'UAR annealing was drastically slower as compared to both 5'UAR/c5'UAR and 5'cHP/c5'cHP annealing and no increase in donor emission was observed even after 12 hours (Fig. S1E). This indicates that the kinetic barrier during the extended duplex ($ED_{3'UAR}$) formation for 5'UAR/3'UAR annealing is considerably higher as compared to both 5'UAR/c5'UAR and 5'cHP/c5'cHP annealing. This higher kinetic barrier also points towards the partial non-complementarity between 5'UAR and 3'UAR hairpins during 5'UAR/3'UAR annealing (Fig. S1B). Due to the extremely slow reaction kinetics of 5'UAR/3'UAR annealing, no kinetic parameters could be determined, at least under our experimental conditions (Fig. S1E).

DENV2C accelerates all three 5'UAR/c5'UAR, 5'cHP/c5'cHP and 5'UAR/3'UAR annealing

To understand the RNA chaperone activity of DENV2C and its role in genome recombination, we characterized the annealing of 5'UAR/c5'UAR, 5'cHP/c5'cHP and 5'UAR/3'UAR in the presence of DENV2C. However, RNA chaperones are known to cause nucleic acid aggregation [31,32,38–40] which can result in fast kinetics that cannot be reliably measured (Fig. S5C) using fluorescence-based techniques [38,41]. Thus, we first determined non-aggregating experimental conditions. Nucleic acid aggregation by positively charged proteins is concentration dependent [30,42] and can be investigated using FCS [31,32]. In FCS, the fluorescence intensity arising from confocal volume (about 0.2 fL) is autocorrelated to obtain information about the processes that give rise to fluorescence fluctuations. These fluctuations are governed by the diffusion of fluorescent species in the confocal volume, and thus parameters like average number of fluorescent species and their diffusion constant can be determined. Aggregation of labelled 5'UAR molecules by the DENV2C would decrease the number of fluorescent oligoribonucleotides (ORNs), N and increase the diffusion time, τ_D . By adding increasing concentrations of DENV2C to labelled ORN or labelled DENV2C, we found no change in N or τ_D up to a DENV2C:ORN molar ratio of 2:1, indicating that no aggregation occurred under these conditions (Fig. S5A and S5B). The optimized annealing reaction performed at a DENV2C:ORN molar ratio of 2:1 at 20°C allowed reliable and reproducible determination of kinetic parameters (further explanations about aggregation conditions are provided in Fig. S5). Thus, we selected a DENV2C:ORN molar ratio of 2:1 to characterize the annealing of 5'UAR/c5'UAR, 5'cHP/c5'cHP and 5'UAR/3'UAR in the presence of DENV2C.

Addition of DENV2C to the labelled 5'UAR or 5'cHP sequences did not lead to any significant change in their fluorescence spectrum (compare black and grey emission spectra in Fig. 3B,C), indicating that DENV2C was unable to destabilize the stem of their secondary structures, similar to other RNA chaperones [31,32]. Annealing of 5'UAR/c5'UAR, 5'cHP/c5'cHP and 5'UAR/3'UAR were then performed by adding DENV2C at a protein to ORN molar ratio of 2:1, to ensure aggregation-free conditions. Interestingly, DENV2C caused a dramatic increase in all the three annealing reactions,

as both 5'UAR/c5'UAR and 5'cHP/c5'cHP annealing were completed much faster as compared to their respective annealing in the absence of the protein (Fig. S1D and S1F). Unlike in the absence of DENV2C, 5'UAR/3'UAR annealing was completed in ~1 hour in the presence of the protein (Fig. 2C and S3E). The kinetic traces could be adequately fitted with Equation (1) and kinetic parameters were obtained for DENV2C-promoted 5'UAR/c5'UAR, 5'cHP/c5'cHP and 5'UAR/3'UAR annealing (Table 1).

Similar to the absence of DENV2C, the fast component, k_{obs1} , varied linearly and the slow component, k_{obs2} , showed hyperbolic dependence with increasing [c5'UAR] during DENV2C-promoted 5'UAR/c5'UAR annealing (Fig. 2E and 2H). This suggests a similar reaction mechanism as to that proposed by Scheme 1. Thus, similar to other RNA chaperone-promoted ORN annealing [32,43] and taking acquired kinetic data into account, a reaction mechanism with single kinetic pathway involving a single 5'UAR/DENV2C complex ($5'UAR_1$) can be proposed:

where a fast pre-equilibrium intermediate complex, $IC_{5'UAR_1}$, precedes the formation of the final stable extended duplex, $ED_{5'UAR_1}$, through a monomolecular reaction [29]. The formation of $IC_{5'UAR_1}$ is governed by the second order association constant, k_{ass} , and the first order dissociation constant, k_{diss} , whereas the formation of $ED_{5'UAR_1}$ is governed by the forward interconversion kinetic rate constant, k_f . Again, we validated 5'UAR/c5'UAR annealing mechanism in the presence of DENV2C by using the Dynafit numerical resolution software (Table S1) [31–35].

To gain further insight into the annealing mechanism, we evaluated the temperature dependence of the k_{obs} values. The relationship revealed positive enthalpy values of the transition states of 28.6 (\pm 0.9) kcal/mol and 18.1 (\pm 1.1) kcal/mol for the fast and slow components, respectively (Fig. 4 and Table 2). These values indicate that 5'UAR/c5'UAR annealing promoted by the DENV2C involves pre-melting of ~5 to ~3 bp in the 5'UAR hairpin structure [36,37].

Next, the linear and the hyperbolic dependence of k_{obs1} and k_{obs2} , respectively with increasing [c5'cHP] (Fig. S4F and S4H) during DENV2C-promoted 5'cHP/c5'cHP annealing implies that the reaction mechanism follows a single kinetic pathway scheme with an accumulation of IC_{cHP1} followed by its interconversion from ED_{cHP1} , similar to the one proposed by scheme 1 (Scheme b in the supplementary). DENV2C-promoted 5'UAR/3'UAR annealing also showed linear and hyperbolic dependence of k_{obs1} and k_{obs2} , respectively with increasing [3'UAR] (Fig. 2F,I), again indicating a reaction scheme similar to that of scheme 1 (Scheme c in the supplementary).

A comparison of the association constants, k_{ass} , suggests DENV2C chaperones the rate of intermediate complex formation by ~2 orders of magnitude during both 5'UAR/c5'UAR and 5'cHP/c5'cHP annealing (Table 1). Similarly, in the presence of DENV2C, the rate of intermediate complex conversion to the extended duplex increases by ~5-folds for 5'UAR/c5'UAR annealing and by ~20-folds for 5'cHP/c5'cHP annealing (comparing corresponding k_f values in Table 1). Interestingly, we observed a ~5-fold increase in the k_{ass} values of the 5'UAR/3'UAR ($39.4 \times 10^3 \text{ M}^{-1}\text{s}^{-1}$) annealing as compared to the k_{ass} value of the 5'UAR/c5'UAR ($8.4 \times 10^3 \text{ M}^{-1}\text{s}^{-1}$) annealing in the presence of DENV2C.

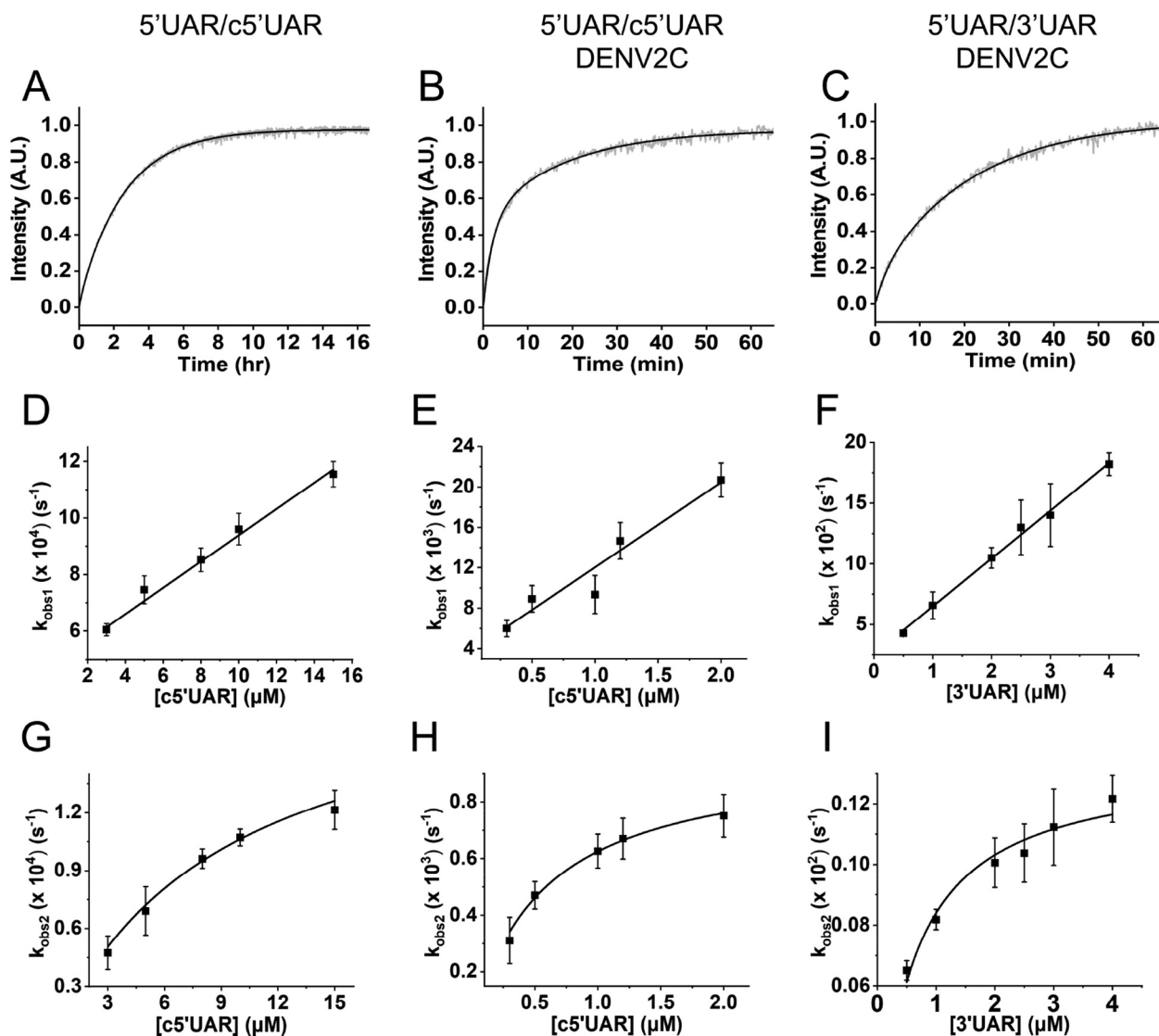


Figure 2. Real-time progress curves (A-C) and kinetic parameters (D-I) of annealing between 5'UAR and its complementary sequences (c5'UAR and 3'UAR) in the presence and absence of DENV2C. (A-C) Real-time progress curves (grey) and their fits to Equation (1) (black) to obtain fast (k_{obs1}) and slow (k_{obs2}) kinetic parameters. Real-time progress curve of the annealing between (A) 10 nM 5'UAR and 8 μ M c5'UAR (B) 10 nM 5'UAR and 1 μ M c5'UAR in the presence of DENV2C with DENV2C: ORN ratio of 2:1 and (C) 10 μ M 5'UAR and 1 μ M 3'UAR in the presence of DENV2C with DENV2C:ORN ratio of 2:1. The obtained values of k_{obs1} and k_{obs2} for (D and G) 5'UAR/c5'UAR, (E and H) 5'UAR/c5'UAR in presence of DENV2C and (F and I) 5'UAR/3'UAR in presence of DENV2C were plotted against corresponding complementary ORNs and fitted to Equation (2) and (3), respectively. Excitation and emission wavelengths used were 480 nm and 520 nm, respectively. Error bars show standard deviation from at least three repeats.

This indicates that the presence of DENV2C probably lowers the kinetic barrier, present due to the non-complementary intermolecular base pairs between 5'UAR and 3'UAR hairpins (Fig. S1B). This result is also in line with the lower enthalpy values obtained for the transition states of 8.2 (\pm 0.4) kcal/mol for the fast component (Fig. 4 and Table 2) during DENV2C-promoted 5'UAR/3'UAR annealing and implies that the formation of IC_{3'UAR1} requires the pre-melting of only \sim 2 bp (Scheme c in the supplementary) as compared to the \sim 5 bp during the formation of IC_{5'UAR1} (Table 1 and Scheme 2). Although IC_{3'UAR1} formed rapidly as compared to IC_{5'UAR1}, the \sim 8-folds increase in its dissociation rate constant, k_{diss} showed that the structural stability of such intermediate complex is substantially low, probably due to the intermolecular base pair mismatches in the

5'UAR/3'UAR duplex as compared to the 5'UAR/c5'UAR duplexes (Fig. S1A and S1B).

DENV2C switches nucleation of 5'UAR/c5'UAR and 5'cHP/c5'cHP annealing through kissing-loop intermediates to stem-stem interactions but not for 5'UAR/3'UAR annealing

We characterize the molecular mechanisms of 5'UAR/c5'UAR and 5'cHP/c5'cHP annealing by investigating the role of the hairpin loop. To determine whether annealing was nucleated through kissing-loop intermediates, we used 5'UAR-Uloop and 5'cHP-Uloop mutants, where the G₉, C₁₀, A₁₁, G₁₂, A₁₃ and A_{10, 11, 12 and 13}, C₁₄ residues, respectively, were changed

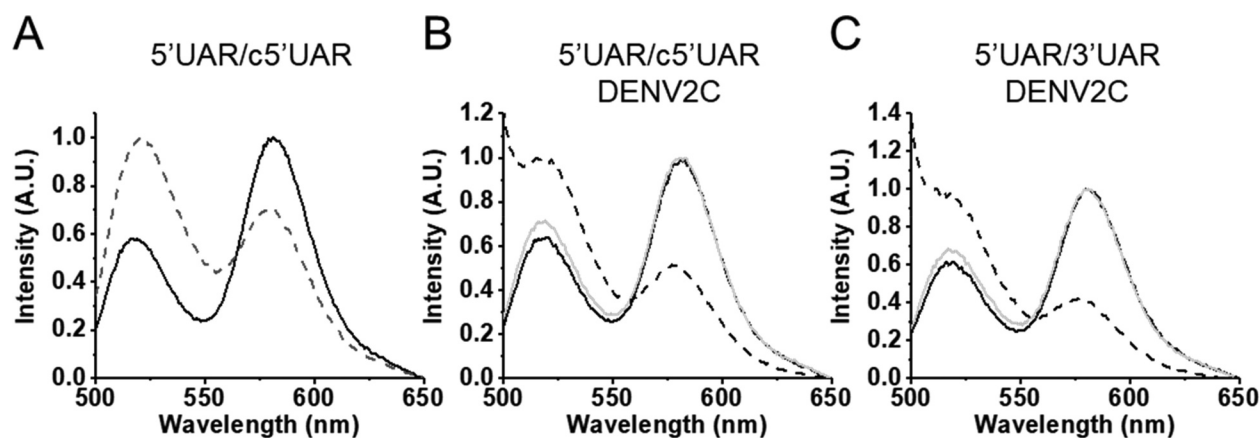


Figure 3. Emission spectra of 5'UAR before (solid black) and after annealing (dotted black) to its complementary sequences. (A) Emission spectra before and after annealing of 10 nM 5'UAR to 8 μ M c5'UAR. (B) Emission spectra of 5'UAR in the absence (solid black) and presence (solid grey) of DENV2C in a DENV2C:ORN ratio of 2:1. The emission spectra after annealing of 10 nM 5'UAR to 1 μ M c5'UAR in the presence of DENV2C is shown in dotted lines. (C) Emission spectra of 5'UAR in the absence (solid black) and presence (solid grey) of DENV2C in a DENV2C:ORN ratio of 2:1. The emission spectra after annealing of 10 nM 5'UAR to 3 μ M 3'UAR in the presence of DENV2C is shown in dotted lines. The excitation wavelength was 480 nm.

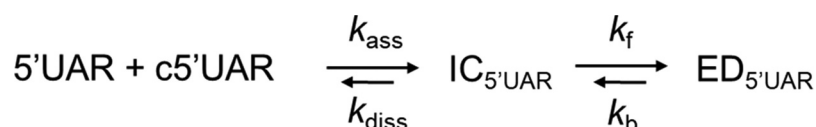
Table 1. Kinetic parameters of 5'UAR/c5'UAR, 5'cHP/c5'cHP and 5'UAR/3'UAR annealing and their mutants in the absence and presence of DENV2C. Kinetic rate constants were calculated from the dependence of k_{obs} values on the concentration of the unlabelled ORN. The k_{ass} and k_{diss} values were calculated with Equation (2), while the K_a and k_f values were calculated using Equation (3). The K_a values were found to differ by a factor of <1.5 from the k_{ass}/k_{diss} values, which further supports the proposed reaction Scheme 1 and 2.

Doubly labelled ORN	Complementary ORN	DENV2C:ORN ratio	k_{ass} ($M^{-1}s^{-1}$) $\times 10^{-3}$	k_{diss} (s^{-1}) $\times 10^4$	K_a (M^{-1}) $\times 10^{-5}$	k_f (s^{-1}) $\times 10^4$
5'UAR	c5'UAR	0	0.05 (± 0.003)	3.6 (± 0.7)	1.11 (± 0.19)	2.02 (± 0.17)
5'UAR	c5'UAR	2	8.4 (± 1.3)	35 (± 15)	16.8 (± 5.1)	9.6 (± 1.1)
5'UAR	3'UAR	2	39.4 (± 1.7)	255 (± 32)	16.9 (± 2.7)	13.4 (± 0.53)
5'cHP	c5'cHP	0	0.085 (± 0.005)	2.6 (± 0.03)	2.3 (± 0.4)	0.5 (± 0.04)
5'cHP	c5'cHP	2	7.4 (± 0.8)	67 (± 9)	16 (± 4)	10.2 (± 1)

to U residues (Fig. 1B) in order to decrease the complementarities between the central loops. For both 5'UAR-Uloop/c5'UAR and 5'cHP-Uloop/c5'cHP annealing reactions, no increase in FAM fluorescence was observed (Fig. 5A and Fig. S6A). This drastic decrease in annealing reactions with the loop mutants strongly suggest that both 5'UAR/c5'UAR and 5'cHP/c5'cHP annealing reactions are mainly nucleated through the kissing-loop intermediates. In contrast, in the presence of DENV2C both 5'UAR-Uloop/c5'UAR and 5'cHP-Uloop/c5'cHP kinetic reactions were found to be similar to that of DENV2C-promoted 5'UAR/c5'UAR and DENV2C-promoted 5'cHP/c5'cHP annealing (Fig. 5B and Fig. S6B), respectively. No decrease in annealing reaction rates (values provided in Fig. 5 legend) with the loop mutants indicate that the role of hairpin loops in DENV2C-promoted 5'UAR/c5'UAR and DENV2C-promoted 5'cHP/c5'cHP annealing is limited and hence, both kinetic reactions are prominently nucleated through the stems. Interestingly, it

was observed that even in aggregation conditions of DENV2C:ORN of 10:1, the annealing mechanism of 5'UAR/c5'UAR and 5'UAR/3'UAR remained predominantly via stem-stem and kissing-loop interactions respectively (Fig. S6C and S6D).

Taken together, these results showed that DENV2C switches the annealing mechanism of RNA elements, 5'UAR and 5'cHP, during (+)/(-) ds-RNA formation from predominantly through kissing-loop intermediates to stem-stem interactions. It is possible that hydrogen bond melting in the stem region of the 5'UAR or c5'cHP hairpin increases due to its interaction with DENV2C protein, and this leads to the switching of the annealing mechanism. Interestingly, a drastic decrease in DENV2C-promoted 5'UAR-Uloop/3'UAR annealing was observed as compared to its counterpart, DENV2C-promoted 5'UAR/3'UAR annealing (Fig. 5C). The result indicates a vital role of the hairpin loop in DENV2C-promoted 5'UAR/3'UAR annealing. Taken



Scheme 1

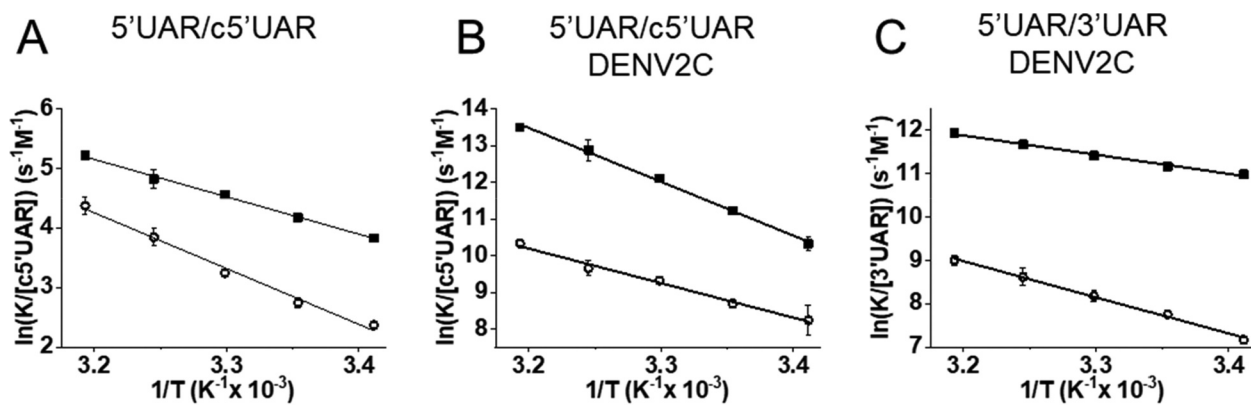


Figure 4. Temperature dependence of 5'UAR/c5'UAR and 5'UAR/3'UAR annealing in the (A) absence and (B and C) presence of DENV2C. The reactions between (A) 10 nM 5'UAR and 10 μ M c5'UAR, (B) 10 nM 5'UAR and 500 nM c5'UAR in the presence of DENV2C and (C) 10 nM 5'UAR and 500 nM 3'UAR in the presence of DENV2C were monitored at various temperatures (20°C, 25°C, 30°C, 35°C and 40°C) to obtain fast, k_{obs1} and slow, k_{obs2} reaction rates. Natural logarithms of the fast (solid squares) and slow (open circles) reaction rates were plotted against the inverse of temperature. Solid lines are fits to Equation (5). The E_a obtained from fitting were used to calculate transition state enthalpies (Table 2) using $\Delta H = E_a - RT$ with $T = 293.15$ K. Excitation and emission wavelengths were 480 nm and 520 nm, respectively. Error bars represent the standard deviations of at least three repeats.

Table 2. Arrhenius parameters of 5'UAR/c5'UAR, 5'cHP/c5'cHP and 5'UAR/3'UAR annealing and their mutants in the absence and presence of DENV2C. The values of the transition state enthalpies, ΔH for the fast and slow pathways were calculated from the fits of temperature dependence of reaction rates, k_{obs} , values to Equation (5), as described in Fig. 4.

Doubly labelled ORN	Complementary ORN	DENV2C: ORN ratio	ΔH (Fast) (kcal/mol)	ΔH (Slow) (kcal/mol)
5'UAR	c5'UAR	0	11.9 ± 0.4	18.0 ± 1.0
5'UAR	c5'UAR	2	28.6 ± 0.9	18.1 ± 1.1
5'UAR	3'UAR	2	8.2 ± 0.4	16.0 ± 0.6

together, the result states that although DENV2 accelerates 5'UAR/3'UAR annealing, the role of the hairpin loop remains crucial during annealing. Thus, the annealing of 5'UAR with its complementary sequence during (+) RNA circularization, 3'UAR, predominantly propagates through loop intermediates. Overall, the results suggest that DENV2C altered the role of hairpin loops in annealing pathways of 5'UAR/c5'UAR and 5'cHP/c5'cHP as compared to their annealing in absence of the protein but not for the 5'UAR/3'UAR annealing. Whilst beyond the scope of the present study, it would be of interesting to quantify the role of hairpin stems in the annealing pathways.

DENV2C protein facilitates 5'UAR/c5'UAR and 5'UAR/3'UAR annealing by decreasing the intrinsic dynamics of the 5'UAR hairpin

To further understand how DENV2C chaperones 5'UAR/c5'UAR and 5'UAR/3'UAR annealing during (+)/(-) ds-RNA formation and (+) RNA circularization respectively, we measured the intrinsic dynamics of 5'UAR in the presence and absence of the protein. We used FRET-FCS [44,45] which analyses the fluctuations in FRET efficiency, caused by doubly labelled 5'UAR conformational fluctuations. Unlike FCS, FRET-FCS measures the proximity ratio (p), which is a function related to FRET efficiency [45–50] and depends on the separation between donor and acceptor but not on the position of the molecules in the observation volume. Thus, the

correlation function of the proximity ratio p (Gp) provides information about structural dynamics of the various 5'UAR conformations. In this case, the 5'UAR might exist in closed, partially-open and fully-open hairpin conformations and thus, the correlation function of p can be fitted to a stretched exponential equation (Fig. 6). The equation provides an effective relaxation time (τ_p), and a stretch parameter (β) describing the heterogeneity of the system. A value of 1 for β indicates that the system displays normal two-state Arrhenius kinetics, with one discrete energy barrier, while a value of 0 for β indicates a continuum of equal energy barriers. The approach was calibrated as mentioned by Sharma KK et al. [49] and effective relaxation time (τ_p) associated with the motion of the 5'UAR hairpin extremities, were determined. Addition of DENV2C to the 5'UAR hairpin resulted in a ~ 2 -fold increase in τ_p (from 74 ± 21 μ s in the absence to 135 ± 28 μ s in the presence of DENV2C) (Fig. 6A), suggesting the hampered fluctuation of 5'UAR hairpin extremities. The β values of 0.21 (± 0.04) in the absence and 0.25 (± 0.06) in the presence of DENV2C showed that the 5'UAR hairpin exists in more than 2 conformations and that the addition of DENV2C does not alter heterogeneity of the system. However, it is possible that one of the 5'UAR hairpin conformations is favoured in the presence of the protein.

We investigated the notion of the favoured 5'UAR conformation among its various conformations using trFRET. In trFRET, the energy transfer from donor to acceptor influences the donor fluorescence lifetime, τ , in a distance-dependent manner. The closer the donor and acceptor dyes are, the faster the donor dye relaxes to ground state and the shorter the lifetime. The fluorescence of 5'UAR had an average lifetime of 1.7 ± 0.2 ns (Fig. 6B) and was best fitted with three discrete lifetime components of ~ 4.3 ns ($\langle \tau_1 \rangle$), ~ 1.9 ns ($\langle \tau_2 \rangle$) and ~ 0.19 ns ($\langle \tau_3 \rangle$) having populations of $31 \pm 5\%$ (α_1), $11 \pm 4\%$ (α_2) and $59 \pm 10\%$ (α_3), respectively (Fig. 6C and 6D). Note that we cannot exclude the existence of conformations with very short lifetimes or with lifetimes close to the three principal components. Those would not be resolvable within our experimental conditions. We refer to the fluorescence lifetime

of closed, partially-open and fully-open conformations of the 5'UAR hairpins as $\langle\tau_3\rangle$, $\langle\tau_2\rangle$ and $\langle\tau_1\rangle$ and their corresponding populations as α_3 , α_2 and α_1 .

No or marginal difference in the average lifetime of the donor was observed after addition of DENV2C to the 5'UAR hairpin. However, a ~ 2 -fold increase in the value of α_2 from $11 \pm 4\%$ to $22 \pm 3\%$ was observed that happened at the expense of both α_1 and α_3 populations (Fig. 6C). The α_1 and α_3 populations showed a decrease from $31 \pm 5\%$ to $24 \pm 4\%$ and from $59 \pm 10\%$ to $54 \pm 9\%$ respectively. The result indicates that as an RNA chaperone with the ability to both dissociate and anneal RNA [20], DENV2C could be effectively unwinding high FRET populations ($\langle\tau_1\rangle$ and α_1) and annealing low FRET populations ($\langle\tau_3\rangle$ and α_3) to allow the 5'UAR hairpin to reach its most favoured kinetic conformation ($\langle\tau_2\rangle$ and α_2). Overall, the results from FRET-FCS and trFRET explain that DENV2C probably exerts its RNA chaperone activities on the 5'UAR by modulating its intrinsic dynamics as well as by decreasing kinetically trapped unfavourable conformations. Such mechanistic behaviour of the DENV2C is in line with the 'entropy exchange model' in which a highly flexible protein, like DENV2C, undergoes disordered-to-ordered transition upon binding to RNA, that in turn leads to the melting of the RNA structure through an entropy exchange process [23].

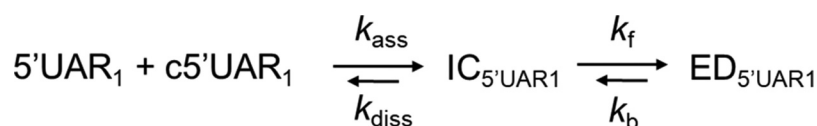
Discussion

The annealing reaction of the essential RNA element, 5'UAR, propagates through kissing-loop intermediates, albeit rather slowly, taking several hours to reach completion (Fig. 2A and

Fig. S1A). This slow annealing kinetics can be related to the requirement of complementary sequences to be in a reactive conformation and proper orientation in order to nucleate the intermediate complex. The melting of two base pairs near the bottom of the 5'UAR are associated with $IC_{5'UAR}$ formation. The $IC_{5'UAR}$ is then converted into the $ED_{5'UAR}$ in a rate limiting step associated with the transition enthalpy of ~ 18 kcal mol $^{-1}$, that likely corresponds to the melting of the three next base pairs in the middle region of the 5'UAR stem. This melting is probably the bottleneck for the interconversion into $ED_{5'UAR}$ (Fig. 7A).

Interestingly, in the presence of DENV2C, the annealing mechanism of 5'UAR/c5'UAR switched from mainly nucleating through kissing-loop intermediates and proceeded via stem-stem interactions. Formation of 5'UAR/c5'UAR intermediates in the presence of DENV2C probably involves melting of the five base pairs in the lower 5'UAR stem and the intermediate complex ($IC_{5'UAR1}$) could be stabilized by up to 10 intermolecular base pairs (Fig. 7B). Moreover, the ~ 5 -fold increased interconversion rate of $IC_{5'UAR1}$ probably results from its stability due to the larger number of intermolecular base pairs and/or more favourable conformation for the subsequent conversion into the $ED_{5'UAR1}$.

In contrast, the vital role of the loop in DENV2C-promoted 5'UAR/3'UAR annealing forced the reaction mechanism to proceed through the kissing-loop intermediate, $IC_{3'UAR1}$. Thus, similar to the 5'UAR/c5'UAR intermediates in the absence of the protein, the formation of 5'UAR/3'UAR intermediates involves melting two base pairs in the upper region of the 5'UAR stem and the resulting intermediate complex could be stabilized by up to eight intermolecular base pairs followed by its



Scheme 2

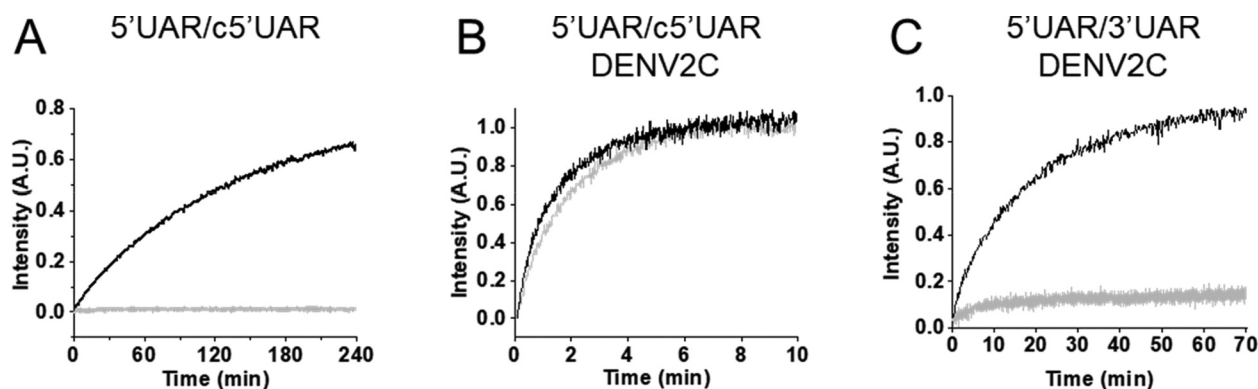


Figure 5. Real-time progress curves of the 5'UAR mutants. Progress curve of dual-labelled 5'UAR (black) or 5'UAR-ULoop mutant (grey) with its complementary sequences (A and B) c5'UAR or (C) 3'UAR in the absence and presence of DENV2C, respectively. (A) 10 μ M c5'UAR, (B) 700 nM c5'UAR and (C) 1 μ M 3'UAR were used for the annealing reaction with either 10 nM of 5'UAR (black traces) or 10 nM of 5'UAR-ULoop (grey traces). (B) Fitting of the progressive curves using Equation (1) provided values for the 5'UAR/c5'UAR reaction in the absence (k_{obs1} and k_{obs2} are $4.0 \times 10^{-2} s^{-1}$ and $4.4 \times 10^{-3} s^{-1}$) and the presence (k_{obs1} and k_{obs2} of $4.5 \times 10^{-2} s^{-1}$ and $4.7 \times 10^{-3} s^{-1}$) of DENV2C. Excitation and emission wavelengths used were 480 nm and 520 nm, respectively.

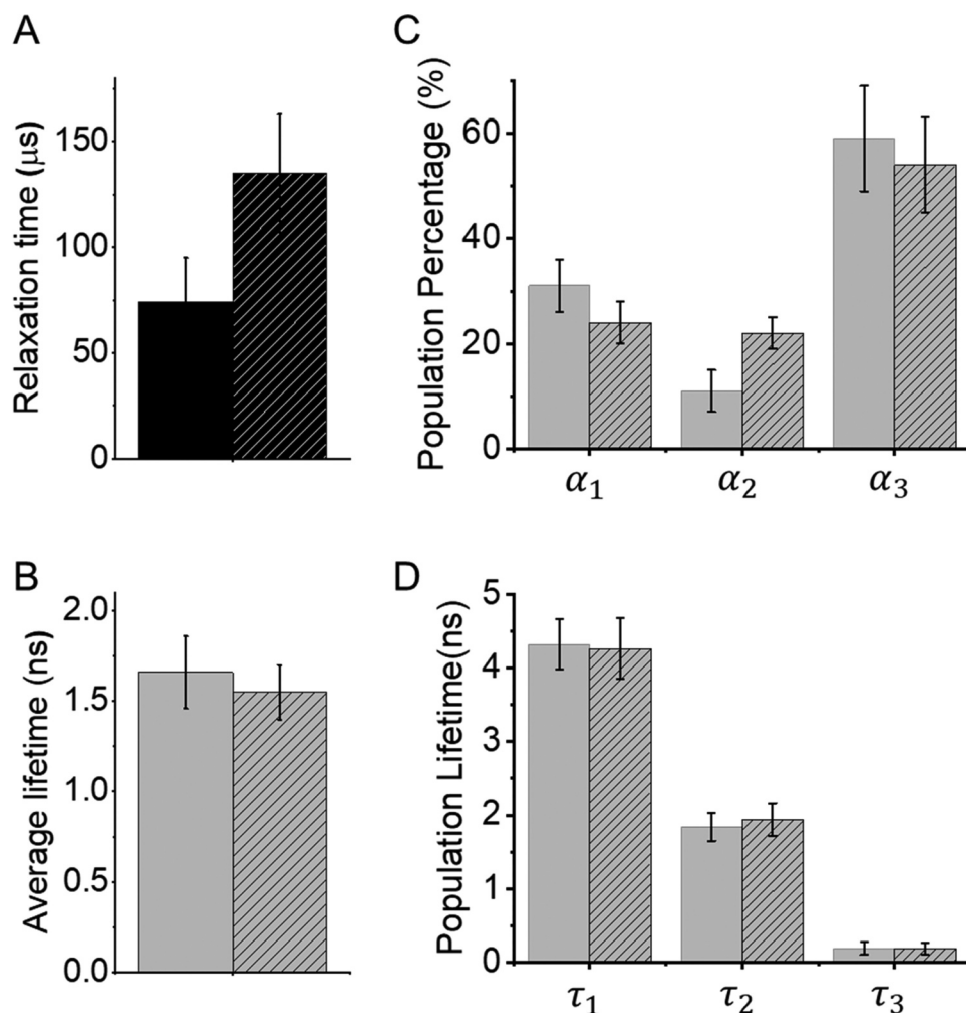


Figure 6. FRET-FCS and trFRET of 5'UAR in the presence and the absence of DENV2C.

(A) The relaxation time, τ_p , of 5'UAR in the absence (solid) and presence (striped) of DENV2C. An autocorrelation function of proximity ratio, $G_p(\tau)$, was constructed using: $G_p(\tau_p) = \frac{\delta P(\tau)\delta P(\tau+\tau_p)}{\langle P(\tau) \rangle^2}$ and fitted to a stretched exponential equation [47]: $G_p(\tau_p) = G_p(0)\exp\left[-\left(\frac{\tau}{\tau_p}\right)^\beta\right]$, where τ_p corresponds to the effective relaxation time associated with the correlated motion and β is a stretch parameter. (B) The lifetime traces for doubly labelled 5'UAR were fitted to a tri-exponential decay model and the average fluorescence lifetimes ($\langle \tau_i \rangle$) of FAM for donor were calculated in the (solid) absence and in the (striped) presence of DENV2C. (C and D) Fitting of the fluorescence decay provided three discrete lifetimes, τ_1 , τ_2 and τ_3 with the corresponding fraction of each population as α_1 , α_2 and α_3 , respectively in the (solid) absence and (striped) the presence of DENV2C added at protein:ORN ratio of 2:1. Error bars represent standard deviations of at least three repeats.

interconversion to the extended duplex by the melting of the next three base pairs in the middle region of the 5'UAR stem (Fig. 7C). The initial three bp at the 5' end of the 5'UAR stem are non-complementary to the corresponding nucleotides in the 3'UAR stems (Fig. S1B). This may hinder the propagation of DENV2C-promoted 5'UAR/3'UAR annealing through the hairpin stems. In addition, the lower transition enthalpy of ~ 8 kcal mol $^{-1}$ (Table 2) indicated a rapid formation of IC $_3$ UAR $_1$ and in turn a ~ 5 -fold increased association constant compared to DENV2C-promoted 5'UAR/c5'UAR annealing (Table 1). However, IC $_3$ UAR $_1$ is probably stabilized with only ~ 5 intermolecular base pairs (involving A $_8$, G $_9$, C $_{10}$, A $_{11}$ and G $_{12}$ of 5'UAR hairpin) which lead to its ~ 8 -fold increased dissociation rate constant compared to the DENV2 promoted 5'UAR/c5'UAR annealing (Table 1). Apart from reduced intermolecular base pairing, the inferior stability of IC $_3$ UAR $_1$ could also be attributed to non-complementarities at the bottom of the 5'UAR loop involving G $_7$ and $_{12}$ (Fig. S1B) and melting of three base pairs in the stable 5'UAR stem. Therefore, the combination

of mismatches defining the stability of the ORN duplexes and the structured RNA elements chaperoned by DENV2C during ORN annealing (either hairpin loop or hairpin stem) probably dictates the processes of annealing of RNA elements representing (+)/(-) ds-RNA formation and (+) RNA circularization.

Our trFRET data showed that DENV2C functions similarly to other RNA chaperones [19,51–56] by binding to RNA, allowing them to escape thermodynamically stable, but possibly non-functional states and thus, explore other states that could be functional [57]. A comparison between different RNA chaperones suggests that DENV2C, HIV-1 NCp7 and hepatitis C virus (HCV) core protein accelerates annealing of complementary ORNs up to 2 to 3 orders of magnitude [31,32,58], indicating similar chaperoning potential for the three proteins. However, DENV2C accelerates annealing of complementary ORNs at two equivalent of protein molecule while HIV-1 NCp7 and HCV core require ~ 6 and ~ 2 equivalent of protein molecules, respectively, to show similar chaperone potential. This suggests that one molecule of either DENV2C or HCV core could be as

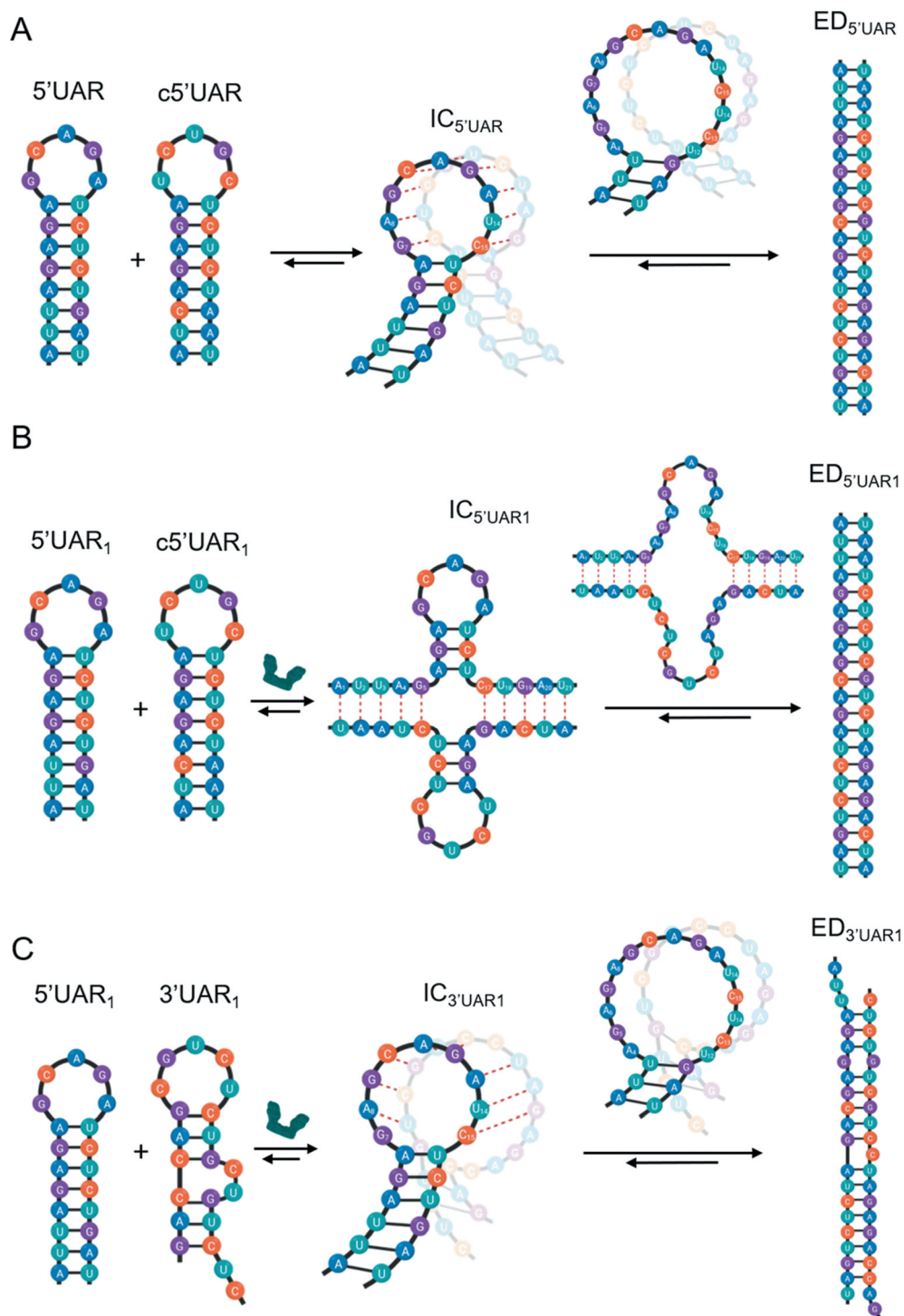


Figure 7. Proposed reaction mechanisms for annealing of 5'UAR/c5'UAR and 5'UAR/3'UAR in presence and absence of DENV2C. (A) Elucidating the proposed mechanism for 5'UAR/c5'UAR annealing involves first, the annealing kinetics showing an accumulation of an intermediate complex ($IC_{5'UAR}$) and thus, suggesting a one-pathway reaction scheme. Annealing is nucleated via a kissing-loop intermediate ($IC_{5'UAR}$), consisting of hydrogen bonding between complementary nucleotides in the loops of the 5'UAR and the c5'UAR (red dashed line). Formation of $IC_{5'UAR}$ involves melting of two base pairs (G_7-C_{15} and A_8-U_{14}) near the bottom of the 5'UAR loop. After which, interconversion from $IC_{5'UAR}$ to $ED_{5'UAR}$ takes place, likely involving the melting of the next three base pairs (A_6-U_{16} , G_5-C_{17} and A_4-U_{18}) in the middle region of the 5'UAR stem. (B) DENV2C-promoted 5'UAR/c5'UAR annealing starts with the opening of the 5'UAR hairpin in the stem region, allowing annealing via the stems. Formation of $IC_{5'UAR1}$ involves melting of the five base pairs (A_1-U_{21} , U_2-A_{20} , U_3-G_{19} , A_4-U_{18} and G_5-C_{17}) in the lower 5'UAR stem. Interconversion from $IC_{5'UAR1}$ to $ED_{5'UAR1}$ involves melting of the three remaining base pairs (A_6-U_{16} , G_7-C_{15} and A_8-U_{14}) in the upper part of 5'UAR stem. (C) DENV2C-promoted 5'UAR/3'UAR annealing takes place predominantly through the kissing-loop intermediates, with $IC_{3'UAR1}$ formation likely involving the melting of the two base pairs (G_7-C_{15} and A_8-U_{14}) near the bottom of the 5'UAR loop. Interconversion from IC to ED likely involves the melting of the three remaining base pairs (A_6-U_{16} , G_5-C_{17} and A_4-U_{18}) in the middle region of the 5'UAR stem.

active as three molecules of HIV-1 NCp7. Interestingly, both DENV2C and HCV core are existing as homodimers while HIV-

1 NCp7 is a monomeric protein *in vitro* [59,60]. Thus, like HCV core, the superior chaperone activity of DENV2C compared to

HIV-1 NCp7 is likely a consequence of the stronger ‘nucleic acid aggregating’ properties, in line with the efficient oligonucleotide aggregation observed by FCS (Fig. S5). This propensity of the DENV2C to neutralize the negatively charged nucleic acids and to promote their aggregation is probably related to the highly flexible and unstructured helix 1 [22,59,61] as compared to the folded HIV-1 NCp7 structure with two zinc fingers [60,62]. Moreover, HIV-1 NCp7 promotes ORN annealing through kissing loop intermediates [29] while the HCV core mainly chaperone the annealing through the stems [31], the DENV2C can propagate annealing either through kissing-loop intermediates (for 5'UAR/3'UAR) or through the stems (for 5'UAR/c5'UAR and 5'cHP/c5'cHP). Taken together, our results show that the DENV2C has stronger nucleic acid annealing activity at low protein:ORN ratios when compared to HIV-1 NCp7, and it can modulate annealing pathways when compared to HCV core. Despite the structural differences between these three proteins, the conserved nucleic acid chaperone properties suggest that they are required in different viruses, in line with the conservation of RNA chaperoning in *Flaviviridae* core proteins [21].

Such properties are not observed in other DENV proteins. Other viral proteins which are essential for RNA replication are NS5 polymerase and NS3 helicase. However, the ribozyme activity assay showed that both NS5 polymerase and NS3 helicase have no or limited RNA chaperoning activity [20]. Another viral protein, NS2A is also shown to interact with RNA. However, NS2A is proposed to be involved in virion assembly, by recruiting the genome via binding to 3'UTR [63]. Since these tested viral RNA-interacting proteins, including DENV2C, are targeting the same RNA in carrying out their functions, it is conceivable that the RNA affinity of these proteins is regulated in maintaining the balance between different events in the viral life cycle. However, DENV2C is likely to be the only viral protein responsible for preventing misfolding of RNA during replication. In addition, there is a possibility of DENV2C playing a role in modulating (+)/(-) ds-RNA formation and (+) RNA circularization by controlling the annealing mechanisms of essential RNA elements. These abilities of DENV2C may be critical for genomic RNA dimerization in DENV replication and RNA packaging as well as in facilitating recombination between various DENV genotypes and subtypes to increase viral variability.

Disclosure statement

The authors declare no conflict of interest.

Funding

This work was supported by the Competitive Research Programme from the National Research Foundation, Singapore under Grant (NRF-CRP19-2017-03-00). X. E. Yong was supported by the NUS Graduate School for Integrative Sciences and Engineering Scholarship; National Research Foundation Singapore [NRF-CRP19-2017-03-00].

ORCID

Xin Ee Yong  <http://orcid.org/0000-0002-4235-0071>

References

- [1] Dowd KA, Pierson TC. The many faces of a dynamic virion: implications of viral breathing on flavivirus biology and immunogenicity. *Annu Rev Virol.* 2018;5:185–207.
- [2] Martina BEE, Koraka P, Osterhaus ADME. Dengue virus pathogenesis: an integrated view. *Clin Microbiol Rev.* 2009;22:564–581.
- [3] Cahour A, Falgout B, Lai CJ. Cleavage of the dengue virus polyprotein at the NS3/NS4A and NS4B/NS5 junctions is mediated by viral protease NS2B-NS3, whereas NS4A/NS4B may be processed by a cellular protease. *J Virol.* 1992;66:1535–1542.
- [4] Edgil D, Polacek C, Harris E. Dengue virus utilizes a novel strategy for translation initiation when cap-dependent translation is inhibited. *J Virol.* 2006;80:2976–2986.
- [5] Edgil D, Harris E. End-to-end communication in the modulation of translation by mammalian RNA viruses. *Virus Res.* 2006;119:43–51.
- [6] Polacek C, Friebe P, Harris E. Poly(A)-binding protein binds to the non-polyadenylated 3' untranslated region of dengue virus and modulates translation efficiency. *J Gen Virol.* 2009;90:687–692.
- [7] Alvarez DE, Filomatori CV, Gamarnik AV. Functional analysis of dengue virus cyclization sequences located at the 5' and 3'UTRs. *Virology.* 2008;375:223–235.
- [8] Filomatori CV, Lodeiro MF, Alvarez DE, et al. A 5' RNA element promotes dengue virus RNA synthesis on a circular genome. *Genes Dev.* 2006;20:2238–2249.
- [9] Alvarez DE, Lodeiro MF, Luduena SJ, et al. Long-range RNA-RNA interactions circularize the dengue virus genome. *J Virol.* 2005;79:6631–6643.
- [10] Hahn CS, Hahn YS, Rice CM, et al. Conserved elements in the 3' untranslated region of flavivirus RNAs and potential cyclization sequences. *J Mol Biol.* 1987;198:33–41.
- [11] Khromykh AA, Meka H, Guyatt KJ, et al. Essential role of cyclization sequences in flavivirus RNA replication. *J Virol.* 2001;75:6719–6728.
- [12] Villordo SM, Gamarnik AV. Genome cyclization as strategy for flavivirus RNA replication. *Virus Res.* 2009;139:230–239.
- [13] Clyde K, Barrera J, Harris E. The capsid-coding region hairpin element (cHP) is a critical determinant of dengue virus and West Nile virus RNA synthesis. *Virology.* 2008;379:314–323.
- [14] Clyde K, Harris E. Secondary RNA. Structure in the coding region of dengue virus type 2 directs translation start codon selection and is required for viral replication. *J Virol.* 2006;80:2170–2182.
- [15] Friebe P, Harris E. Interplay of RNA elements in the dengue virus 5' and 3' ends required for viral RNA replication. *J Virol.* 2010;84:6103–6118.
- [16] Yu L, Nomaguchi M, Padmanabhan R, et al. Specific requirements for elements of the 5' and 3' terminal regions in flavivirus RNA synthesis and viral replication. *Virology.* 2008;374:170–185.
- [17] Filomatori CV, Iglesias NG, Villordo SM, et al. RNA sequences and structures required for the recruitment and activity of the dengue virus polymerase. *J Biol Chem.* 2011;286:6929–6939.
- [18] S.M. Villordo, D.E. Alvarez, A. V. Gamarnik, A balance between circular and linear forms of the dengue virus genome is crucial for viral replication, *Rna.* 2010;16:2325–2335. DOI:10.1261/rna.2120410
- [19] Herschlag D. RNA chaperones and the RNA folding problem. *J Biol Chem.* 1995;270:20871–20874.
- [20] Pong WL, Huang ZS, Teoh PG, et al. RNA binding property and RNA chaperone activity of dengue virus core protein and other viral RNA-interacting proteins. *FEBS Lett.* 2011;585:2575–2581.
- [21] Ivanyi-Nagy R, Lavergne JP, Gabus C, et al. RNA chaperoning and intrinsic disorder in the core proteins of Flaviviridae. *Nucleic Acids Res.* 2008;36:712–725.
- [22] Ma L, Jones CT, Groesch TD, et al. Solution structure of dengue virus capsid protein reveals another fold. *Proc Natl Acad Sci U S A.* 2004;101:3414–3419.
- [23] Tompa P, Csermely P. The role of structural disorder in the function of RNA and protein chaperones. *Faseb J.* 2004;18:1169–1175.
- [24] Boon PLS, Saw WG, Lim XX, et al. Partial intrinsic disorder governs the dengue capsid protein conformational ensemble. *ACS Chem Biol.* 2018;13:1621–1630.

- [25] Kuhn RJ, Zhang W, Rossmann MG, et al. Structure of dengue virus: implications for flavivirus organization, maturation, and fusion. *Cell*. 2002;108:717–725.
- [26] Sangiambut S, Keelapang P, Aaskov J, et al. Multiple regions in dengue virus capsid protein contribute to nuclear localization during virus infection. *J Gen Virol*. 2008;89:1254–1264.
- [27] Martins IC, Gomes-Neto F, Faustino AF, et al. The disordered N-terminal region of dengue virus capsid protein contains a lipid-droplet-binding motif. *Biochem J*. 2012;444:405–415.
- [28] Boudier C, Storchak R, Sharma KK, et al. The mechanism of HIV-1 Tat-directed nucleic acid annealing supports its role in reverse transcription. *J Mol Biol*. 2010;400:487–501.
- [29] Vo MN, Barany G, Rouzina I, et al. HIV-1 nucleocapsid protein switches the pathway of transactivation response element RNA/DNA annealing from loop-loop “kissing” to “zipper.”. *J Mol Biol*. 2009;386:789–801.
- [30] Bloomfield VA, He S, Li AZ, et al. Light scattering studies on DNA condensation. *Biochem Soc Trans*. 1991;19:496.
- [31] Sharma KK, Didier P, Darlix JL, et al. Kinetic analysis of the nucleic acid chaperone activity of the hepatitis C virus core protein. *Nucleic Acids Res*. 2010;38:3632–3642.
- [32] Sharma KK, De Rocquigny H, Darlix JL, et al. Analysis of the RNA chaperoning activity of the hepatitis C virus core protein on the conserved 3'X region of the viral genome. *Nucleic Acids Res*. 2012;40:2540–2553.
- [33] Sharma KK, Przybilla F, Restle T, et al. Reverse transcriptase in action: FRET-based assay for monitoring flipping and polymerase activity in real time. *Anal Chem*. 2015;87:7690–7697.
- [34] Sharma KK, Przybilla F, Restle T, et al. FRET-based assay to screen inhibitors of HIV-1 reverse transcriptase and nucleocapsid protein. *Nucleic Acids Res*. 2016;44:e74.
- [35] Kuzmič P. Program DYNAFIT for the analysis of enzyme kinetic data: application to HIV proteinase. *Anal Biochem*. 1996;237:260–273.
- [36] Rouzina VA, Bloomfield, Heat capacity effects on the melting of DNA. I. General aspects. *Biophys J*. 1999;77:3242–3251. DOI:10.1016/S0006-3495(99)77155-9
- [37] Cantor CR, Schimmel PR. *Biophysical chemistry: part II: techniques for the study of biological structure and function*. Macmillan; 1980.
- [38] Egelé C, Piémont E, Didier P, et al. The single-finger nucleocapsid protein of moloney murine leukemia virus binds and destabilizes the TAR sequences of HIV-1 but does not promote efficiently their annealing. *Biochemistry*. 2007;46:14650–14662.
- [39] Stewart-Maynard KM, Cruceanu M, Wang F, et al. Retroviral nucleocapsid proteins display nonequivalent levels of nucleic acid chaperone activity. *J Virol*. 2008;82:10129–10142.
- [40] Cristofari, JL Darlix. The ubiquitous nature of RNA chaperone proteins. *Prog Nucleic Acid Res Mol Biol*. 2002; 72:223–268. DOI:10.1016/s0079-6603(02)72071-0.
- [41] J Godet, H de Rocquigny, C Raja, N Glasser, D Ficheux, J-L Darlix, Y Mély, During the Early Phase of HIV-1 DNA Synthesis, Nucleocapsid Protein Directs Hybridization of the TAR Complementary Sequences via the Ends of their Double-stranded Stem. *J Mol Biol*. 2006;356:1180–1192. DOI:10.1016/j.jmb.2005.12.038
- [42] Stoylov SP, Vuilleumier C, Stoylova E, et al. Ordered aggregation of ribonucleic acids by the human immunodeficiency virus type 1 nucleocapsid protein. *Biopolymers*. 1997;41:301–312.
- [43] Ramalanjaona N, de Rocquigny H, Millet A, et al. Investigating the mechanism of the nucleocapsid protein chaperoning of the second strand transfer during HIV-1 DNA synthesis. *J Mol Biol*. 2007;374:1041–1053.
- [44] Lim XX, Chandramohan A, Lim XYE, et al. Conformational changes in intact dengue virus reveal serotype-specific expansion. *Nat Commun*. 2017;8. DOI:10.1038/ncomms14339
- [45] Torres T, Levitus M. Measuring conformational dynamics: A new FCS-FRET approach. *J Phys Chem B*. 2007;111:7392–7400.
- [46] Lim XX, Chandramohan A, Lim XYE, et al. Epitope and paratope mapping reveals temperature-dependent alterations in the dengue-antibody interface. *Structure*. 2017;25:1391–1402.e3.
- [47] Wallace ML, Ying L, Balasubramanian S, et al. FRET fluctuation spectroscopy: exploring the conformational dynamics of a DNA hairpin loop. *J Phys Chem B*. 2000;104:11551–11555.
- [48] Sharma KK, Marzinek JK, Tantirimudalige SN, et al. Single-molecule studies of flavivirus envelope dynamics: experiment and computation. *Prog Biophys Mol Biol*. 2019;143:38–51.
- [49] Sharma KK, Lim XX, Tantirimudalige SN, et al. Infectivity of dengue virus serotypes 1 and 2 is correlated with e-protein intrinsic dynamics but not to envelope conformations. *Structure*. 2019;27:618–630.e4.
- [50] Wallace MI, Ying L, Balasubramanian S, et al. Non-arrhenius kinetics for the loop closure of a DNA hairpin. *Proc Natl Acad Sci U S A*. 2001;98:5584–5589.
- [51] Urbaneja MA, Wu M, Casas-Finet JR, et al. HIV-1 nucleocapsid protein as a nucleic acid chaperone: spectroscopic study of its helix-destabilizing properties, structural binding specificity, and annealing activity. *J Mol Biol*. 2002;318:749–764.
- [52] Ermolenko DN, Makhatadze GI. Bacterial cold-shock proteins. *Cell Mol Life Sci*. 2002;59:1902–1913.
- [53] Sasaki K, Kim MH, Imai R. Arabidopsis COLD SHOCK DOMAIN PROTEIN2 is a RNA chaperone that is regulated by cold and developmental signals. *Biochem Biophys Res Commun*. 2007;364:633–638.
- [54] Kang H, Park SJ, Kwak KJ. Plant RNA chaperones in stress response. *Trends Plant Sci*. 2013;18:100–106.
- [55] W Jiang, Y Hou, M Inouye. CspA, the major cold-shock protein of *Escherichia coli*, is an RNA chaperone. *J Biol Chem*. 1997;272:196–202. DOI:10.1074/jbc.272.1.196.
- [56] Schroeder R, Grossberger R, Pichler A, et al. RNA folding in vivo. *Curr Opin Struct Biol*. 2002;12:296–300.
- [57] Rajkowsch L, Chen D, Stampfl S, et al. RNA chaperones, RNA annealers and RNA helicases. *RNA Biol*. 2007;4:118–130.
- [58] Vo MN, Barany G, Rouzina I, et al. Mechanistic studies of mini-TAR RNA/DNA annealing in the absence and presence of HIV-1 nucleocapsid protein. *J Mol Biol*. 2006;363:244–261.
- [59] Jones CT, Ma L, Burgner JW, et al. Flavivirus capsid is a dimeric alpha-helical protein. *J Virol*. 2003;77:7143–7149.
- [60] Summers MF, Henderson LE, Chance MR, et al. Nucleocapsid zinc fingers detected in retroviruses: EXAFS studies of intact viruses and the solution-state structure of the nucleocapsid protein from HIV-1. *Protein Sci*. 1992;1:563–574.
- [61] Faustino AF, Carvalho FA, Martins IC, et al. Dengue virus capsid protein interacts specifically with very low-density lipoproteins. *Biophys J*. 2014;106:388a.
- [62] Morellet N, de Rocquigny H, Mély Y, et al. Conformational behaviour of the active and inactive forms of the nucleocapsid NCp7 of HIV-1 studied by 1H NMR. *J Mol Biol*. 1994;235:287–301.
- [63] Xie X, Zou J, Zhang X, et al. Dengue NS2A protein orchestrates virus assembly. *Cell Host Microbe*. 2019;26:606–622.e8.
- [64] Iglesias NG, Gamarnik AV. Dynamic RNA structures in the dengue virus genome. *RNA Biol*. 2011;8:249–257.